Implication of tidal forcing effects on the zonal variation of solstice equatorial plasma bubbles

Loren C. Chang[1,2], Cornelius Csar Jude H. Salinas[1,2], Yi-Chung Chiu[1,2], McArthur Jones Jr.[3], Chi-Kuang Chao[1,2], Jann-Yenq Liu[1,2], Charles C.H. Lin[4], Tung-Yuan Hsiao [5]

[1]Institute of Space Science and Engineering, National Central University, Taoyuan City, Taiwan.
[2]Center for Astronautical Physics and Engineering, National Central University, Taoyuan City, Taiwan.
[3]Space Science Division, Naval Research Laboratory, MD, USA.
[4]Department of Earth Science, National Cheng Kung University, Tainan, Taiwan.
[5]Institute of Nuclear Engineering and Science, National Tsing Hua University, Hsinchu City, Taiwan.

Key Points:

- EPB variation over Central Pacific and African sectors hypothesized to be caused by tidal forcing.
- COSMIC TEC shows recurrent maximum of wave-2 tidal signatures over both regions at midnight LT.
- Numerical experiments show atmospheric tides can produce a wave-2 pattern in nighttime TEC.

Corresponding author: L. C. Chang, loren@g.ncu.edu.tw

Abstract

Equatorial plasma bubbles (EPBs) are elongated plasma depletions that can occur in the nighttime ionospheric F region, causing scintillation in satellite navigation and communications signals. EPBs are believed to be Rayleigh-Taylor instabilities seeded by vertically propagating gravity waves. A necessary pre-condition for EPB formation is a threshold vertical ion drift from the E region, which is required to produce the vertical plasma gradients conducive to this instability. Factors affecting the variation of EPBs therefore include magnetic declination, the strength of the equatorial electojet, and the wind dynamo in the lower thermosphere controlling vertical plasma drifts. In most longitude zones, this results in elevated EPB occurrence rates during the equinoxes. The notable exception is over the central Pacific and African sectors, where EPB activity maximizes during solstice. *Tsunoda et al.* [2015] hypothesized that the solstice maxima in these two sectors could be driven by a zonal wavenumber 2 atmospheric tide in the mesosphere and lower thermosphere. In this study, we find that the post-sunset electron density observed by FORMOSAT-3/COSMIC during the boreal summer from 2007 - 2012 does indeed exhibit a wave-2 zonal distribution, consistent with results expected from elevated vertical ion drift over the Central Pacific and African sectors. Numerical experiments are also carried out which found that forcing from the aforementioned tidal and stationary planetary wave (SPW) components produced wave-2 modulations on vertical ion drift, ion flux convergence, and midnight TEC. The relation between the vertical ion drift enhancements and the midnight TEC enhancements are consistent with the solstice maxima hypothesis.

1 Introduction

Radio waves propagating through the ionosphere can be refracted and diffracted by the plasma of the Earth's ionosphere. Refraction is caused by changes in phase velocity and the corresponding refractive index, which is is a function of radio frequency, electron density, Earth's magnetic field strength, and collision frequencies. This phenomena is utilized for over the horizon communications using high frequency (HF, 3 - 30 MHz) band radio transmissions. Radio waves at the HF band and frequencies below are reflected or absorbed by the ionosphere [*Frissell et al.*, 2014], leaving higher frequencies for trans-ionospheric radio frequency (RF) applications such as satellite communications and Global Navigation Satellite Systems (GNSS). Nonetheless, irregularities in ionospheric plasma distribution can cause diffraction of these trans-ionospheric RF signals, resulting in rapid fluctuations and fading in the received signal to noise ratio. This phenomena is referred to as scintillation, with severe cases of scintillation capable causing loss of lock on the receiver end, rendering satellite communications and navigation services unusable [*Kelly et al.*, 2014; *Moraes et al.*, 2014; *Jiao and Morton*, 2015]. Understanding the sources, generation mechanisms, and generation preconditions for scintillation causing ionospheric irregularities is therefore of great practical importance.

Scintillation events occurring at various latitudes can be the result of different ionospheric irregularities and can vary in severity. Using ground based GNSS receivers located at various latitudes, *Jiao and Morton* [2015] found that scintillation at low latitudes was typically more severe than that at high latitudes, the latter of which was more sensitive to geomagnetic conditions. This latitudinal variation in scintillation severity and sources was further confirmed by *Xiong et al.* [2016] using Swarm satellite observations, who attributed high latitude scintillation to gradient drift instability and energetic particle precipitation, while low latitude scintillation was driven primarily by equatorial plasma bubbles (EPBs). EPBs are longitudinally narrow but latitudinally long plasma depletions that extend poleward along magnetic field lines from the magnetic equator. In comparison, the longitudinal extent of EPBs is on the order of 200 km or less [*Smith and Heelis*, 2017]. Prediction of EPBs is complicated by the fact that their small longitudinal scales typically fall below the grid sizes of most general circulation models (GCMs), requiring

the use of very fine resolution localized models [*Yokoyama et al.*, 2014]. Nonetheless, GCMs are still valuable for understanding the preconditions favorable for EPB formation and their respective spatial and temporal variation.

The preconditions favorable to EPB occurrence are strongly related to the formation mechanism and physical interpretation. EPBs occur in the post-sunset F region ionosphere, which still retains a comparatively high plasma density compared to the ionospheric layers below, even in the absence of sunlight. This is due to the higher concentration of atomic ions in the F region, which have a longer lifetime compared to the rapid dissociate recombination of the molecular ions that are dominant below. The end result of this difference in plasma recombination rates results in a steep vertical plasma density gradient due to the relatively higher plasma densities in the F region. Perturbations introduced to this statically unstable situation can result in the formation of a Rayleigh-Taylor instability resulting in the rapid depletion of F region plasma along magnetic field lines, thus forming an EPB [*Sultan*, 1996]. Conditions favorable to EPB formation therefore include a large positive vertical plasma gradient in the post-sunset ionosphere. This condition is aided by large vertical plasma drifts exceeding a threshold value, which has been identified as a necessary but not sufficient condition for EPB formation [*Smith et al.*, 2015]. An initial seed perturbation is also necessary to trigger the formation of an EPB, which is thought to be a gravity wave with vertical wavelength sufficiently long to propagate upward into the F region [*Fritts and Alexander*, 2001; *de la Beaujardière et al.*, 2004; *Tsunoda et al.*, 2015].

All of the aforementioned factors contribute to the seasonal, geographical, and solar cycle variation in EPB occurrence, particularly that of the strong post sunset vertical plasma drift and the resulting large positive vertical plasma gradient. The Pre-Reversal Enhancement (PRE) corresponds to such a post-sunset increase in vertical plasma drift conducive to the strong positive vertical plasma density gradients favorable for EPB formation. Numerical experiments from *Fesen et al.* [2000] indicated that the vertical drift resulting from the PRE are directly proportional to solar activity, while being inversely proportionate to nighttime E region electron densities. Much like the PRE, EPBs also have a higher occurrence rate and larger growth rates around the equinoxes in most longitude zones when the terminator is aligned with both ends of magnetic field lines, resulting in similar electrical conductivities and larger vertical ion drift [*Tsunoda*, 1985].

This vertical ion drift precondition and its relation to the angle between the terminator and magnetic field lines therefore imposes a dependence upon both season and magnetic declination on EPB occurrence rates. Defense Meteorological Satellite Program (DMSP) observations by [*Gentile et al.*, 2011] have shown that EPBs occur most frequently around the equinoxes when the terminator and magnetic field lines are aligned in most longitude zones. The exceptions to this are South America, Africa, and the Central Pacific. In the case of South America, EPBs occur most frequently during the boreal summer, due to the larger magnetic declination angles in this sector [*Tsunoda et al.*, 2015]. In the case of Africa and the Central Pacific, EPB occurrence rates and nighttime vertical plasma drifts are highest during the boreal summer, for reasons which are not well understood. The vertical plasma drift in the equatorial ionosphere is known to be driven by atmospheric tides via the E region wind dynamo, capable of modulating the zonal variation of vertical plasma drift [*Immel et al.*, 2006; *Liu and Richmond*, 2013]. *Tsunoda et al.* [2015] noted that the African and Central Pacific sectors were separated by roughly 180 degrees in longitude and hypothesized that the anomalous seasonal variation of the vertical ion drift and EPB occurrences in these two sectors could be caused by forcing from atmospheric tides with zonal wavenumber 2.

In this study, we utilize FORMOSAT-3/COSMIC electron density observations and numerical experiments to determine whether such a wave-2 distribution consistent with the above hypothesis actually exists, as well as whether such a wave-2 distribution can be

Component	Tidal Harmonic (n)	UT Zonal Wavenumber (s)
SPW2	0	2
DW3	1	-3
DE1	1	1
S0	2	0
SW4	2	-4

Table 1. Tidal and SPW components with wave-2 distribution at constant LT.

forced by atmospheric tides in the E region. To our knowledge, this is the first examination of the wave-2 EPB hypothesis using observations and numerical experiments.

2 Methodology

Based on the hypothesis of *Tsunoda et al.* [2015], the boreal summer maxima in EPB occurrence rates in the Central Pacific and African sectors is due to a similar distribution in nighttime vertical ion drift forced by atmospheric tides. We therefore expect to find tidal signatures in ionospheric electron densities exhibiting a wave-2 distribution in constant local time, maximizing above the two aforementioned sectors during local nighttime. We also expect a similar distribution in vertical ion drift when the ionosphere is forced by atmospheric tides exhibiting a wave-2 distribution in constant local time.

The zonal wavenumbers (s) of atmospheric tidal components are typically expressed in a universal time (UT) frame. Based upon the universal time (UT) to local time (LT) conversion of tidal harmonics (n) and zonal wavenumbers described by *Forbes et al.* [2008], the zonal wavenumber of a tidal component in the LT frame is the sum of the tidal harmonic and the UT zonal wavenumber. Tidal and stationary planetary wave (SPW) components exhibiting a wave-2 pattern in the LT frame will thus satisfy the condition:

$$s + n = \pm 2 \tag{1}$$

Tidal and stationary planetary wave (SPW) components satisfying this condition are shown in Table 1, corresponding to SPW2, DW3, DE1, S0, and SW4, hereafter referred to as the "wave-2 components". Note that positive zonal wavenumbers denote eastward propagating tides, while negative zonal wavenumbers denote westward propagating tides. Zonal wavenumber zero denotes a zonally symmetric component.

2.1 FORMOSAT-3 / COSMIC

To determine whether the signatures of the wave-2 atmospheric tidal and SPW components are present in the ionosphere, we utilize electron density observations from FORMOSAT-3/COSMIC (hereafter referred to as COSMIC) from 2007 - 2012. Launched in 2006 into six orbital planes at 800 km altitude and 72° inclination, the six COSMIC microsatellites provide vertical profiles of electron density derived from GPS radio occultation.

The COSMIC electron densities are vertically integrated between 200 - 800 km altitude to yield the total electron content (TEC), that are then binned into a 5° grid in geographic and magnetic apex latitude. The amplitudes and phases of ionospheric tidal and stationary planetary wave component signatures are derived using the methodology of *Chang et al.* [2013a], utilizing a linear least-squares fit applied to a sliding 40-day win-

dow centered on each day from 2007 - 2012. The 40 day window ensures coverage over all local times during this time period [*Chang et al.*, 2013b], while also acting to smooth the temporal variation of tidal amplitudes and phases [*Häusler et al.*, 2015].

The derived amplitudes and phases of the tidal and SPW ionospheric signatures will be used to examine whether the seasonal and longitudinal variation of the post-sunset ionosphere is consistent with the hypothesized wave-2 distribution with nighttime peaks in electron density over the African and Central Pacific sectors. Per the methodology of *Chang et al.* [2013a] and *Chang et al.* [2013b], the daily absolute TEC amplitudes at each latitude are normalized by the daily maximum zonal mean TEC in the equatorial region. The use of these normalized amplitudes allows for the solar cycle variation in absolute amplitude to be suppressed, while at the same time allowing for the daily latitudinal variation of each component to be preserved without convolution with the latitudinal variation in zonal mean TEC.

2.2 TIE-GCM

To determine whether the wave-2 atmospheric tides can introduce a corresponding zonal modulation of vertical ion drift and electron density, we perform a series of numerical experiments using the National Center for Atmospheric Research (NCAR) Thermosphere Ionosphere Electrodynamics General Circulation Model (TIE-GCM). TIE-GCM is a fully nonlinear general circulation model of the thermosphere and ionosphere with a lower boundary near 97 km, and an upper boundary between approximately 500 - 1000 km depending upon the solar activity level. The entire model is subject to solar and geomagnetic inputs, while the effects of atmospheric tides propagating into the thermosphere from the middle and lower atmosphere are accounted for using specified tidal climatologies at the lower boundary. Detailed descriptions of TIE-GCM can be found in *Roble et al.* [1988] and *Richmond et al.* [1992].

For the purposes of our numerical experiments, we utilize TIE-GCM version 2.0 with a horizontal resolution of 2.5° in latitude and longitude, as well as a vertical resolution of four points per scale height. To account for potential differences in different tidal climatogies, the atmospheric tides at the lower boundary are specified using two separate climatologies in two separate sets of numerical experiments: the Global Scale Wave Model 2002 (GSWM-02) and the Climatological Tidal Model of the Thermosphere (CTMT).

GSWM is a mechanistic model that solves the steady state linearized primitive equations subject to specified tidal heating in the lower atmosphere, dissipation in the middle atmosphere, and specified zonal mean zonal wind and temperature fields. Using this method, the amplitudes and phases of several migrating and nonmigrating diurnal and semidiurnal tides can be computed from the surface to an altitude of 124 km. GSWM has been included as the standard tidal lower boundary condition for several past TIE-GCM studies [*Hagan et al.*, 2002, 2003].

Figure 1 shows the temperature amplitudes of GSWM nonmigrating tides corresponding to a wave-2 structure in constant local time at the 97 km TIE-GCM lower boundary as a function of geographic latitude and month. These wave-2 tides include DE1 (Figure 1a), DW3 (Figure 1b), SW4 (Figure 1c), and S0 (Figure 1d), which were included in the lower boundary conditions for the TIE-GCM runs forced by GSWM. It can be seen from the aforementioned figures that DE1, SW4, and S0 all exhibit seasonal maximum during the boreal summer with peak amplitudes in the range of 1.5 - 2 K. DW3 amplitudes exhibit a local minima during this season, but are still in the same amplitude range as the other tidal components. All four tidal components exhibit a distinct latitudinal structure during the boreal summer. DE1 exhibits a bimodal structure in latitude, DW3 exhibits a single peak near the equator, SW4 shows a bimodal structure biased towards the

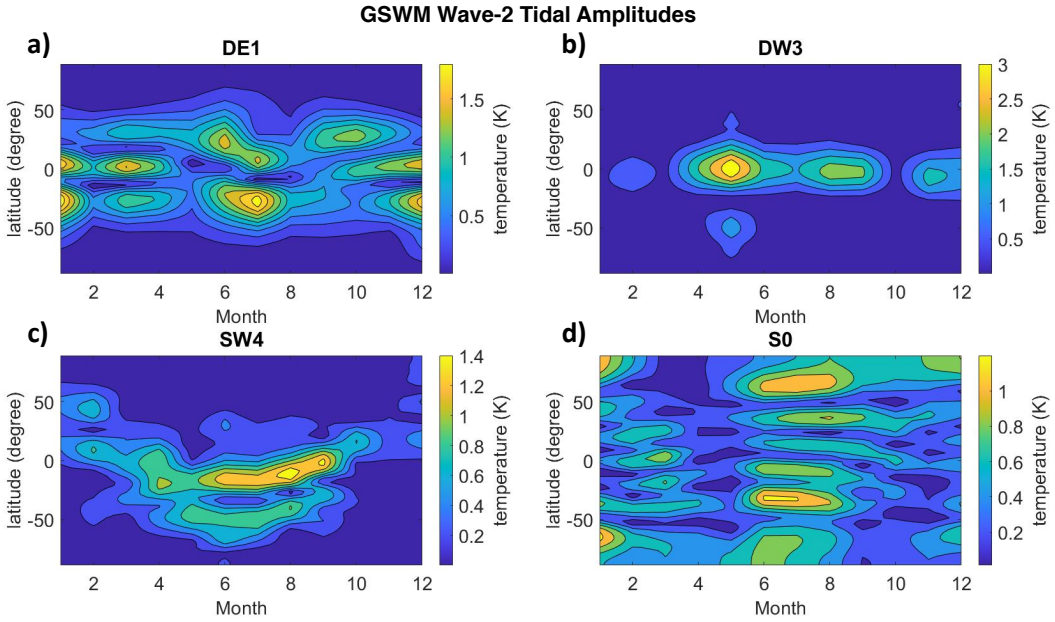

Figure 1. Temperature amplitudes of GSWM wave-2 nonmigrating tides at the TIE-GCM lower boundary as a function of geographic latitude and month for a) DE1, b) DW3, c) SW4, and d) S0.

southern hemisphere, while S0 shows a more complex latitudinal structure with four peaks in the mid to low latitudes and two additional peaks in the high latitudes.

CTMT is a self-consistent climatological model of migrating and nonmigrating atmospheric tides in the thermosphere derived by [*Oberheide et al.*, 2011] through the fitting of Thermosphere Ionosphere Mesosphere Energetics and Dynamics (TIMED) satellite temperature and wind observations to Hough mode extensions extending from 80 - 400 km. In this sense, the amplitudes and phases of the dominant tidal modes are fitted from observations, allowing for values more consistent with actual conditions. The temperature amplitudes of CTMT nonmigrating tides utilized in this study to account for wave-2 effects at the TIE-GCM lower boundary are shown in Figure 2, and include DE1 (Figure 2a), SW4 (Figure 2b), and S0 (Figure 2c). DW3 climatologies are not available from CTMT, and were therefore not included in the lower boundary conditions for the CTMT-forced TIE-GCM runs. First employed by *Jones et al.* [2014], CTMT is now included as a lower boundary tidal option with TIE-GCM version 2.0.

Although there are some similarities with the GSWM wave-2 nonmigrating tides shown previously in Figure 1, there are several striking differences with those resolved in CTMT, likely due to differences in the lower atmospheric tidal sources in GSWM, as well as the background middle atmospheric winds and temperatures that affect tidal propagation and dissipation. In the case of DE1, both CTMT and GSWM resolve a bimodal structure that is quasi-symmetric about the equator with larger amplitudes on the order of 1.5 K during boreal summer. Unlike GSWM, SW4 and S0 in CTMT show generally smaller amplitudes during this time compared to during other times of year. The structure of SW4 in CTMT is again bimodal about the equator, although considerably more symmetric compared to GSWM. While the latitudinal structure of S0 in CTMT is again more complex, there are two peaks in the low to mid latitude region, as opposed to the four resolved in GSWM. Both models show a peak in the high latitudes of both hemispheres during this time. There are also differences in the phases of the wave-2 nonmigrating tides resolved in

Tidal Climatology	Solar Activity	Lower Boundary Condition
GSWM	Low	Migrating Tides Only
		Migrating + Wave-2 Tides
	High	Migrating Tides Only
		Migrating + Wave-2 Tides
CTMT	Low	Migrating Tides Only
		Migrating + Wave-2 Tides
	High	Migrating Tides Only
		Migrating + Wave-2 Tides

Table 2. TIE-GCM runs performed.

both models (not shown). It is expected that these differences in amplitude and phase will manifest in the responses to vertical coupling effects in the ionosphere.

Using each tidal climatology, TIE-GCM was forced using migrating diurnal and semidiurnal tides only (hereafter referred to as the "migrating only runs") or a superposition of the migrating tides and nonmigrating diurnal and semidiurnal tides from Table 1, which correspond to a wave-2 distribution in constant local time (hereafter referred to as the "wave-2 runs"). Each set of runs was further formed for high (Daily and 81-day average $F_{10.7}$ = 200 sfu, cross tail potential = 60 kV, hemispheric power = 39 GW) and low levels (Daily and 81-day average $F_{10.7}$ = 70 sfu, cross tail potential = 30 kV, hemispheric power = 18 GW) of solar activity, resulting in a total of 8 TIE-GCM runs using the different tidal climatologies, lower boundary settings, and solar activity level as tabulated in Table 2.

We note that SPW2 was not included in the numerical experiments as climatologies suitable for use with TIE-GCM are not available. Additionally, SPW2 in the middle atmosphere is associated predominately with Rossby waves occurring in the winter high latitudes surrounding the stratospheric polar vortex, and are filtered by the mean winds at altitudes lower than the ionospheric E region. *Forbes et al.* [2002] noted that SPW2 amplitudes were small above 80 km, suggesting that their effect on transmitting the wave-2 signature via the E region dynamo is much smaller compared to the nonmigrating tides. The GSWM and CTMT lower boundary conditions are identical for both solar maximum and solar minimum conditions.

3 Results

In the following, we present the results of our analysis on the structure and variability of the ionospheric wave-2 in COSMIC observations to determine whether it is consistent with the anomalous seasonal variation in EPBs over the African and Central Pacific sectors. This is followed by the results of the TIE-GCM numerical experiments to determine whether the observed ionospheric features can be generated through tidal forcing as hypothesized.

3.1 Ionospheric Wave-2 Signature Observations

We first seek to examine the seasonal variation and latitudinal structure of the wave-2 component signatures fitted from COSMIC TEC observations to determine whether they are capable of contributing to the boreal maximum in EPB activity over the African and Central Pacific sectors. Figure 3 shows the variation of the wave-2 tidal and SPW component signatures in COSMIC TECs as a function of magnetic latitude and time from 2007

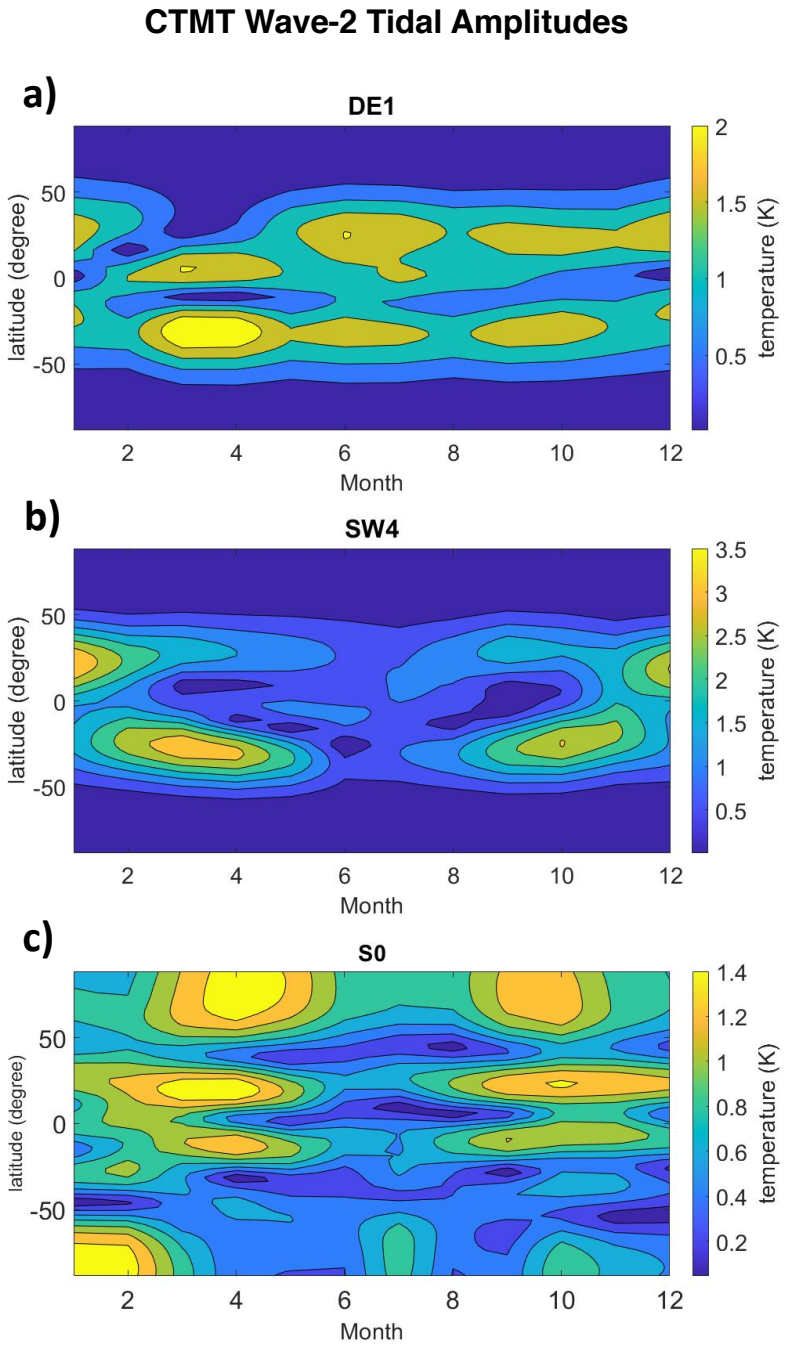

Figure 2. Temperature amplitudes of CTMT wave-2 nonmigrating tides at the TIE-GCM lower boundary as a function of geographic latitude and month for a) DE1, b) SW4, and c) S0.

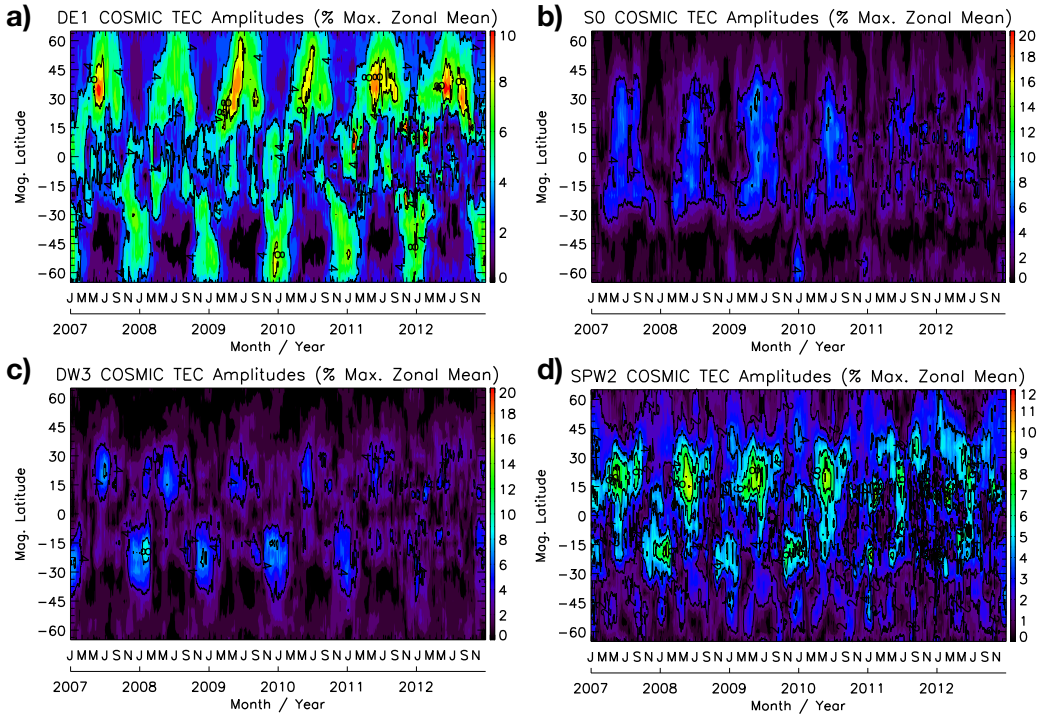

Figure 3. Relative amplitude in COSMIC TEC of a) DE1, b) S0, c) DW3, and d) SPW2 as a function of magnetic latitude and time. Daily fit amplitudes at all latitudes normalized by daily maximum zonal mean.

- 2012. Here, we have identified that the ionospheric tidal components that maximize in the low latitude region during boreal summer, consistent with the anomalous EPB variation in the Central Pacific and African sectors. These components are DE1 (Figure 3a), S0 (Figure 3b), DW3 (Figure 3c), and SPW2 (Figure 3d).

DE1, DW3, and SPW2 maximize between 15°N - 45°N magnetic latitude during the boreal summer, while S0 is quasi-symmetric about the magnetic equator. SW4 (not shown) maximizes during November - December in the southern hemisphere between 15° - 30°S, and is therefore unlikely to contribute to the anomalous EPB variation during the boreal summer. The seasonal and latitudinal variation of these components is interannually recurrent, indicating that these are coherent features of ionospheric variability. The repeated occurrence of the wave-2 components (except SW4) in the low latitude and equatorial regions during the boreal summer indicates that they have the potential to contribute to elevated electron densities in the F region during the nighttime.

We now consider whether the phases of the aforementioned wave-2 tidal component signatures are consistent with elevated electron densities over the African and Central Pacific sectors during boreal summer nighttimes. The spatial features produced by the aforementioned wave-2 components in TEC maximizing during the boreal summer can be seen in Figure 4, which shows the TEC magnitudes reconstructed from the average amplitudes and phases of DE1 (Figure 4a), S0 (Figure 4b), DW3 (Figure 4c), and SPW2 (Figure 4d) during boreal summer 2008 (days 135 - 225) at 00 hours local time (LT) as a function of geographic latitude and longitude. 2008 corresponds to low levels of solar activity.

It can be seen that all four components exhibit midnight maximum in or near the African sector (0° through 45° longitude) in the southern magnetic hemisphere during this time, with DE1 and DW3 showing peaks almost directly over Africa, while S0 and SPW2

show peaks off the African coast over the Indian Ocean. DE1 and DW3 further show maxima in the Central Pacific sector (-180° through -135° longitude), while the peaks of S0 and SPW2 are shifted closer toward the eastern Pacific. A similar geographic distribution can be seen in Figure 5, which shows the local midnight latitude and longitude distribution of DE1 (Figure 5a), S0 (Figure 5b), DW3 (Figure 5c), and SPW2 (Figure 5d) during boreal summer 2011, corresponding to elevated levels of solar activity. DE1 and DW3 again show midnight peaks covering Africa and the Central Pacific, while the peaks of S0 and SPW2 are shifted further eastward.

Expressed in local time, the zonal angular phase velocity of a tidal component can be expressed as:

$$c_{LT} = \frac{n\Omega}{s+n} \tag{2}$$

Here, $\Omega = \frac{360^\circ}{24}$ hour^{-1} is the Earth's angular rotation rate, while positive (negative) values correspond to eastward (westward) zonal phase velocities. Consulting the values in Table 1, the longitudes of the peaks will shift with local time, with DE1 and S0 shifting to the east with local time, and DW3 shifting to the west. The peaks of DE1 will therefore be directly over Africa post-midnight (around 3LT), whereas the peaks of S0 are located directly over Africa pre-midnight (roughly around 19LT). DW3 has one peak almost directly over Africa at 00LT. As the bulk of ionospheric electron density is in the F region during the nighttime, DE1 and DW3 account for a midnight electron density distribution consistent with favorable formation conditions for EPBs in the African and Central Pacific sectors.

Also note that DE1 and SPW2 also produce midnight maximum in the northern hemisphere above Europe and Northeast Asia, consistent with the Mid-Summer Nighttime Anomaly (MSNA) [*Lin et al.*, 2010]. This geographic distribution is consistent in both 2008 and 2011, during low and high levels of solar activity, respectively.

Figure 6 shows the superposition of all COSMIC TEC wave-2 components at 00 LT in the boreal summer of both 2008 (Figure 6a) and 2011 (Figure 6b). It can be seen that for both of these years, as well as all other years examined in this study, the ionosphere wave-2 corresponds to midnight enhancements in TEC above the Central Pacific and African sectors in the southern hemisphere, as well as over Europe and Northeast Asia in the northern hemisphere. The COSMIC observations therefore confirm that an ionospheric wave-2 is indeed present during the boreal summer, with spatial distribution in the southern hemisphere and equatorial region consistent with that which would be expected from enhanced vertical ion drift over Africa and the Central Pacific.

3.2 Tidal Forcing Experiments

We now utilize TIE-GCM to determine whether wave-2 atmospheric tidal components are capable of modulating the nighttime vertical ion drift and electron density, creating regions favorable for EPB occurrence. As shown previously in Table 2, we perform separate TIE-GCM runs with migrating tides only lower boundary conditions (the "migrating only runs"), as well as runs with migrating tides and wave-2 tides at the lower boundary (the "wave-2 runs"). This process is repeated using both GSWM and CTMT tidal climatologies at low and high solar activity.

Figure 7 shows the differences between TIE-GCM parameters from the wave-2 and migrating only model runs at solar maximum in geographic latitude and longitude. The figures in the left column correspond to the model runs using GSWM lower boundary conditions, while the right column corresponds to the model runs using CTMT lower boundary conditions. The top row shows the difference in TEC at 00 LT, while the middle row shows the difference in ion flux convergence vertically integrated between 200 - 400 km at 22 LT, and the bottom row shows the difference between vertical ion drift at 300

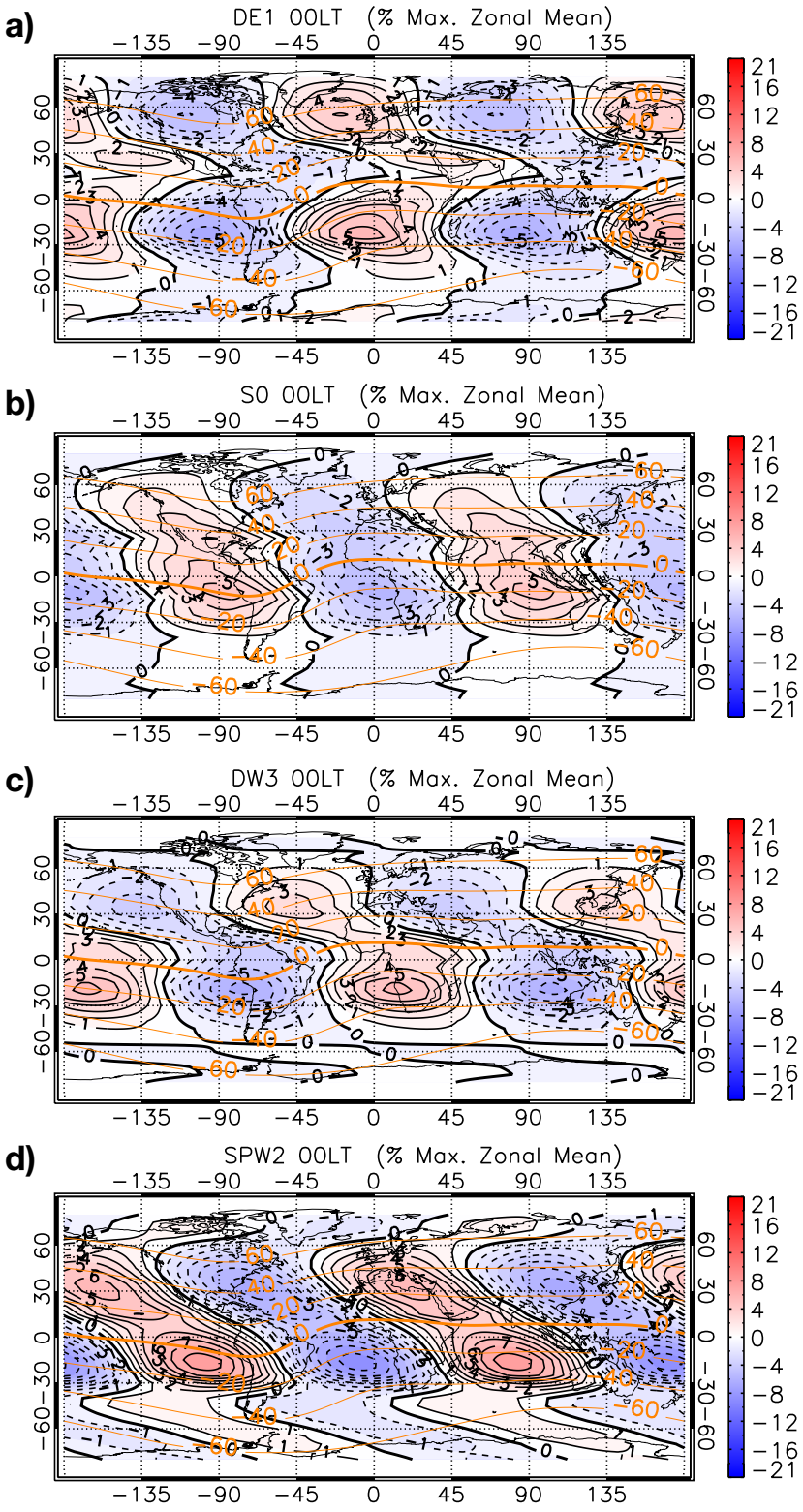

Figure 4. Spatial features produced by COSMIC wave-2 TEC components during boreal summer 2008 at 00 hours local time as a function of latitude and longitude. Components shown are a) DE1, b) S0, c) DW3, and d) SPW2. Magnetic apex latitudes given by orange contours. Magnitudes normalized by maximum zonal mean TEC.

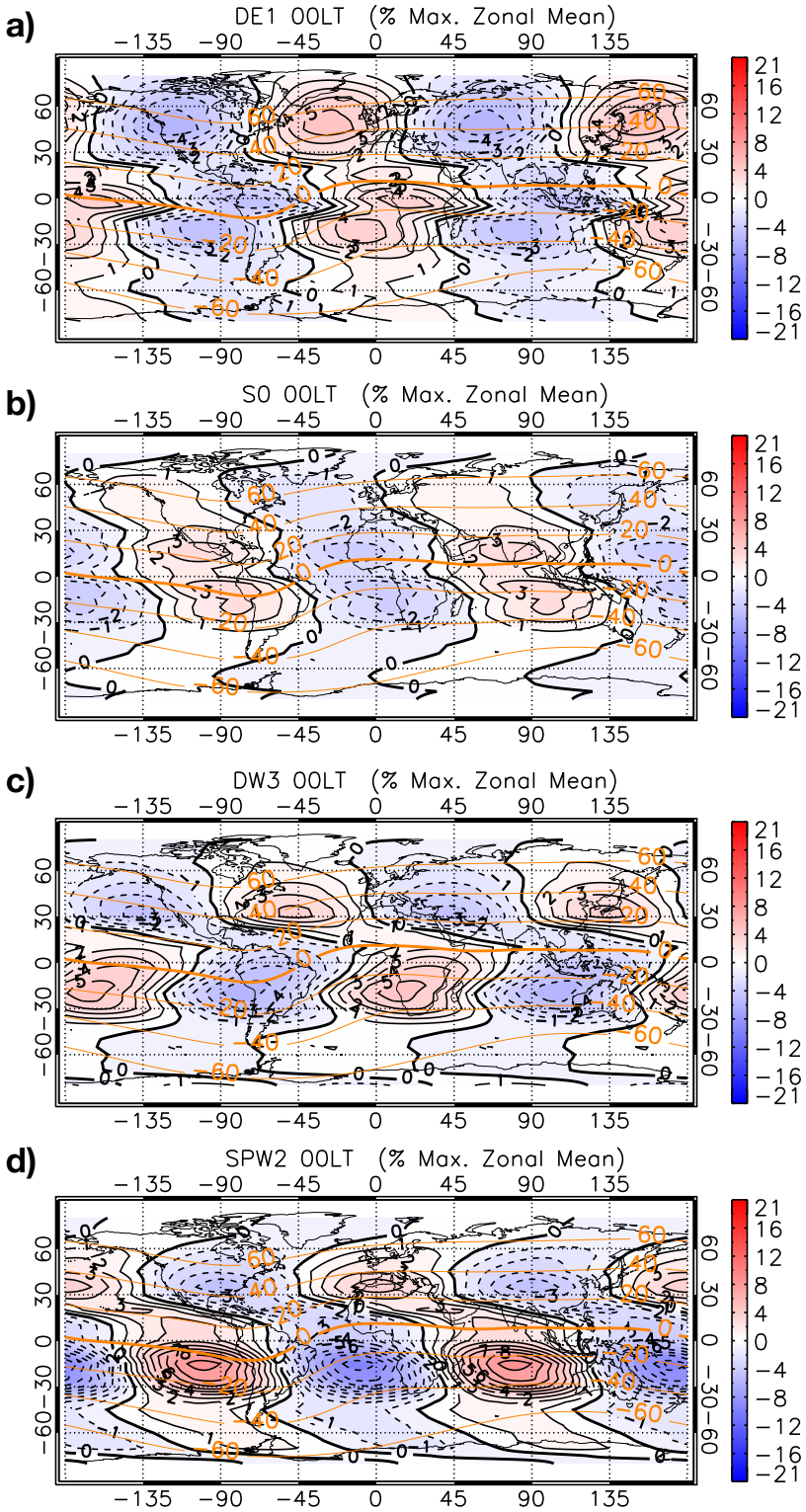

Figure 5. Same as Figure 4, but for 2011

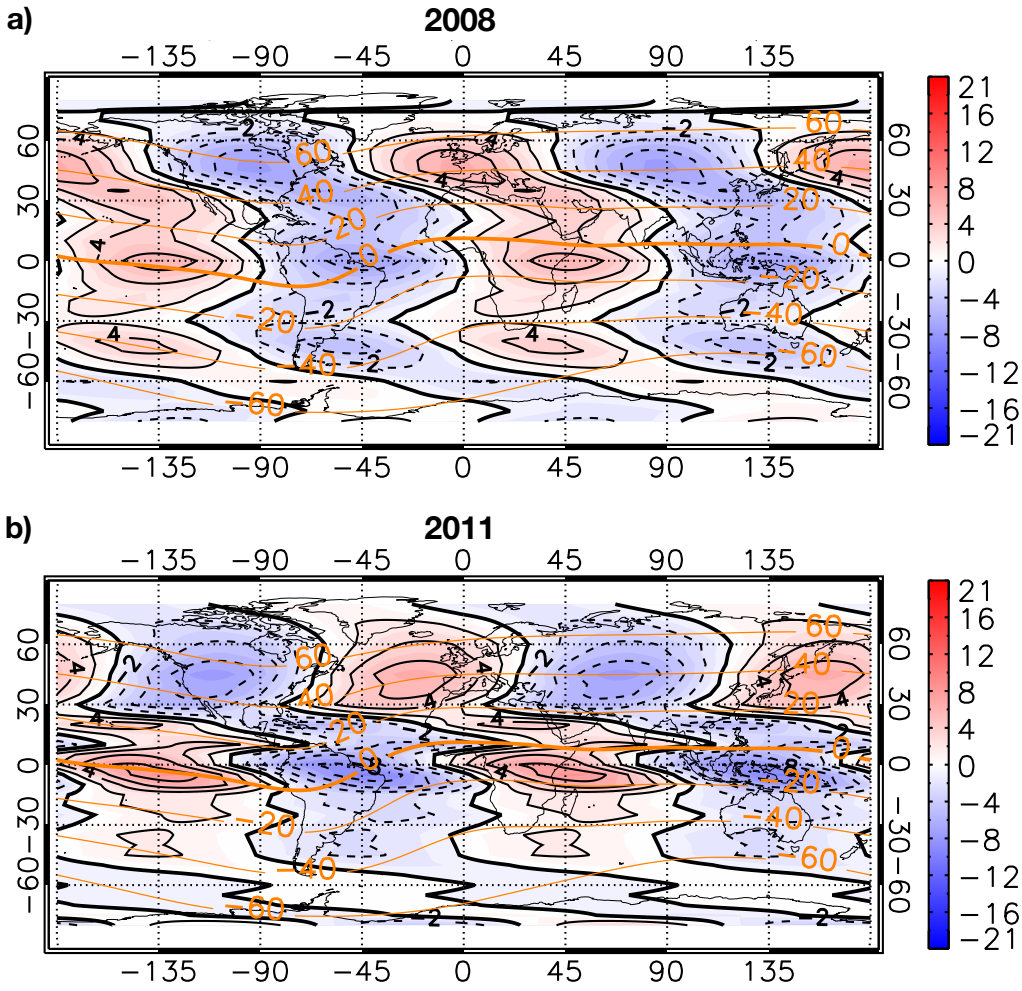

Figure 6. Superposition of all COSMIC TEC wave-2 components at 00 LT as a function of geographic latitude and longitude during the boreal summer of a) 2008 and b) 2011. Magnitudes normalized by maximum zonal mean TEC.

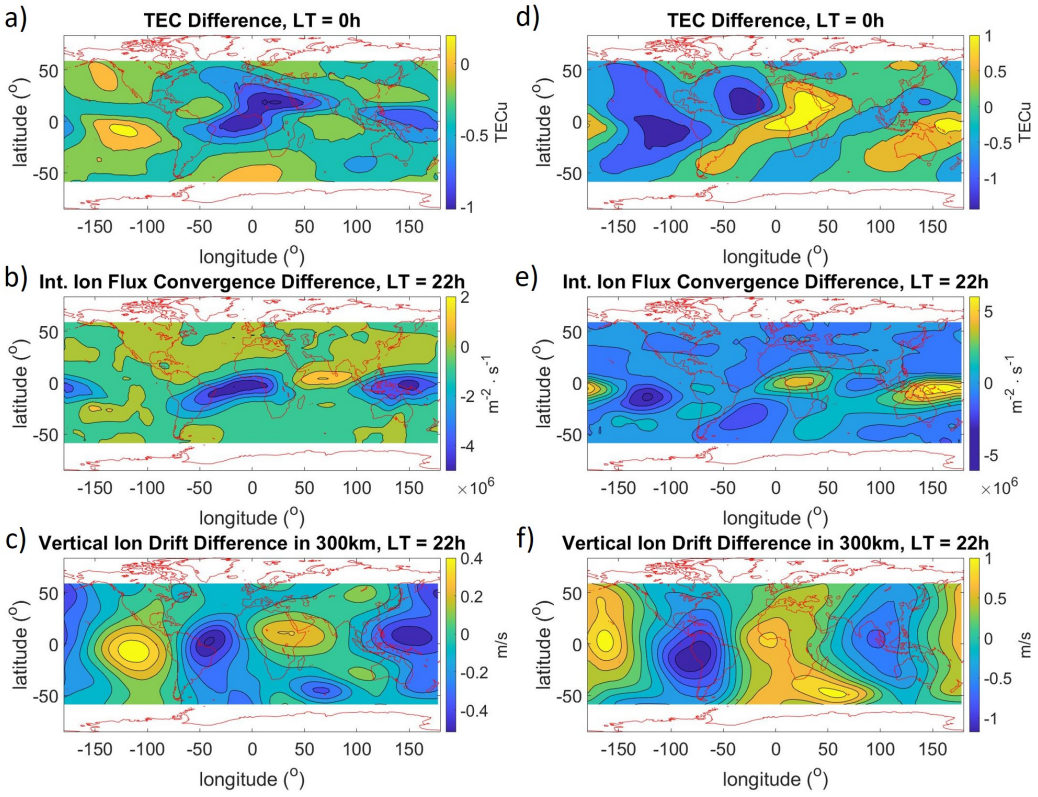

Figure 7. Geographic latitude and longitude maps of difference between TIE-GCM runs with and without GSWM (left column) and CTMT (right column) wave-2 lower boundary conditions at solar maximum for TEC at 00 LT (top row), vertically integrated ion convergence at 22 LT (middle row), and vertical ion drift at 22 LT (bottom row). Note the difference in magnitudes between the GSWM and CTMT runs.

km and 22 LT. The two hour delay between the TEC and ion transport difference fields is to account for the latency between changes in transport and changes in TEC.

From Figure 7a, it can be seen that GSWM wave-2 forcing results in a wave-2 pattern in the TEC difference, albeit with different phases in different latitude zones. In the southern hemisphere tropics, the wave-2 peaks are respectively over the Central Pacific and the Indian Ocean, while the peaks in the northern tropics are shifted to being above South America and East Asia. The former is closer to the 2011 COSMIC observations shown previously in Figure 6b, indicating that there are still differences between wave-2 tidal phases and the corresponding ionospheric changes in the model run and in reality. The aforementioned TEC enhancements over the Central Pacific and Africa are similar to the geographic distribution in low latitude enhancements in integrated ion flux convergence shown in Figure 7b, although the Central Pacific enhancement in integrated flux convergence is shifted to the south of the TEC enhancement. A stronger similarity in spatial distribution is seen with the low latitude enhancements in vertical ion drift shown in Figure 7c, with equatorial enhancements over the Central Pacific, as well as Eastern Africa. The difference in the longitudes of the integrated ion flux convergence wave-2 peak over the Indian Ocean and the vertical ion drift peak over Eastern Africa suggest that horizontal transport may play a larger role in the formation of the TEC wave-2 peak over the Indian Ocean, compared to the Central Pacific wave-2 TEC peak, which can be attributed mostly to changes in vertical drift.

Similarly, a wave-2 pattern is also resolved for the changes in TEC using CTMT wave-2 forcing, shown in Figure 7d, though with phases shifted to the west compared to the GSWM forcing results, as well as with larger magnitudes. In this case, equatorial peaks are resolved over the Western / Central Pacific and Africa. These enhancements in midnight TEC are similar in spatial distribution to the changes in ion flux convergence (Figure 7e) and vertical ion drift (Figure 7f), again demonstrating that wave-2 tidal forcing at the lower boundary of TIE-GCM can result in the generation of a wave-2 in midnight vertical ion drift, TEC and by extension, F-region plasma density.

Ionospheric changes in response to wave-2 forcing at solar minimum are shown in Figure 8. As can be seen in Figures 8a and 8d, a wave-2 pattern is introduced to 00 LT TEC using lower boundary forcing from both GSWM and CTMT wave-2 tides. The longitudes of the enhancements in response to GSWM forcing are shifted considerably from the expected regions, occurring over Central America and East Asia. The CTMT-driven enhancements occur over the African and Central Pacific sectors as expected. Compared to the solar maximum results shown previously in Figure 7, the magnitudes of the wave-2 TEC enhancement are smaller by roughly half. The solar minimum enhancements are also shifted further into the northern hemisphere tropics and subtropics compared to the solar maximum results, as well as the COSMIC observations from 2008 (Figure 4).

The longitudes of the wave-2 enhancements in TEC are consistent with those resolved in vertically integrated ion flux convergence at 22 LT shown in Figures 8b and 8e for GSWM and CTMT, respectively. It is notable that the integrated ion flux convergence enhancements occur closer to the equator compared to the TEC enhancements, with the latter potentially being the result of plasma cascading down along magnetic field lines to higher latitudes. Figure 8c shows the changes in vertical ion drift at 300 km in response to GSWM wave-2 tidal forcing. The longitudes of the vertical ion drift enhancements are displaced to the west of the integrated ion flux convergence enhancements, indicating that horizontal ion transport also plays a role in the formation of the wave-2 TEC enhancements. A larger difference is also resolved between the geographic distribution of the vertical ion drift enhancements compared to that of the integrated ion flux and TEC enhancements in response to CTMT wave-2 tidal forcing shown in Figure 8f.

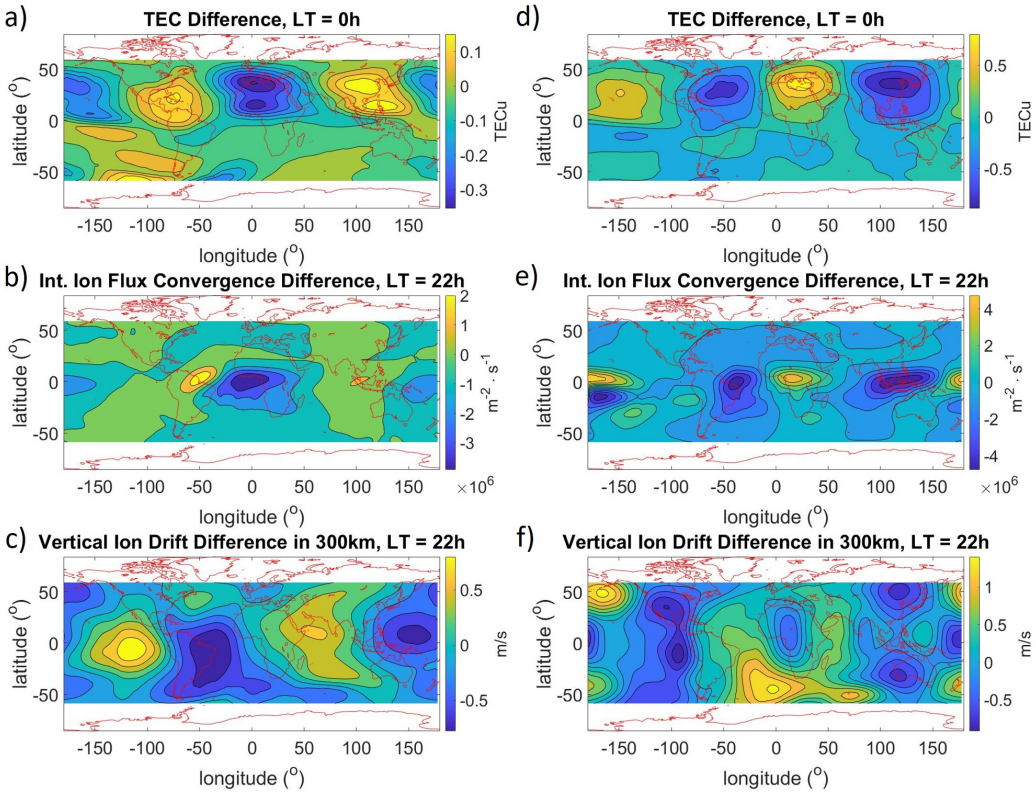

Figure 8. Same as Figure 7, but for solar minimum.

4 Discussion

Taken together, the results of the COSMIC observations show that a wave-2 enhancement in TEC with peaks over the Central Pacific and African sectors at 00 LT is a persistent feature during the boreal summer at both solar maximum and solar minimum. This is consistent with the hypothesis of *Tsunoda et al.* [2015] that the increased plasma bubble occurrence rates during this season over these two sectors can be attributed to higher nighttime F-region plasma densities and vertical gradients. The TIE-GCM numerical experiments demonstrated that forcing from wave-2 atmospheric tides can produce wave-2 enhancements in TEC during both solar maximum and solar minimum conditions. The longitudes of the equatorial wave-2 TEC enhancements resolved using CTMT wave-2 tidal forcing are closer to the expected Central Pacific and African sectors compared to that resulting from GSWM wave-2 tidal forcing. This is consistent with the fact that the CTMT tides are the result of fitting to SABER and TIDI observations, and would therefore be expected to have amplitudes and phases in the lower thermosphere that are closer to reality. The latitudinal structures of the TEC wave-2 resolved in TIE-GCM show greater differences with observations, and may be related to model variables not constrained by observations, such as thermospheric neutral winds, as well as direct propagation of atmospheric tides into the thermosphere.

Although wave-2 TEC enhancements are resolved in response to wave-2 tidal forcing at both solar maximum and solar minimum, there is a greater consistency between the geographic distribution of the vertical ion drift enhancements and the corresponding wave-2 enhancements in integrated ion flux convergence and TEC at solar maximum compared to solar minimum. This suggests that formation of the ionospheric wave-2 in TEC is more strongly dependent on vertical ion drift enhancements, and by extension, wave-2 atmospheric tides modulating the equatorial fountain via the E-region dynamo during solar maximum. At solar minimum, other coupling mechanisms such as horizontal plasma transport or direct propagation of the atmospheric tides may play a larger role. The latter mechanism is consistent with the reduced thermospheric tidal dissipation during solar minimum, which was found by *Oberheide et al.* [2009] to result in significant thermospheric amplitude increases of long vertical wavelength tides such as DE3. We note again that the tidal lower boundary conditions were identical for both solar maximum and solar minimum conditions, which indicates that any differences in the ionospheric wave-2 response can be attributed to in-situ thermosphere and ionosphere mechanisms.

5 Conclusions

Analysis of FORMOSAT-3/COSMIC observations and TIE-GCM numerical experiments were performed to examine the hypothesis of *Tsunoda et al.* [2015], which attributed the elevated plasma bubble occurrence rates during boreal summer over the African and Central Pacific sectors to modulation of vertical plasma drifts resulting from interaction of atmospheric tides of local time zonal wavenumber 2 with the E-region dynamo. This hypothesis is supported by observational results which revealed a recurrent nighttime wave-2 pattern with TEC enhancements over Africa and the Central Pacific during all of the boreal summers from 2007 - 2012, consistent with increased nighttime vertical plasma gradients and plasma bubble growth rates.

Numerical experiments conducted using TIE-GCM forced by wave-2 atmospheric tides from GSWM and CTMT found that the midnight TEC wave-2 can be produced during both solar maximum and solar minimum using this method, with the longitudes of the enhancements formed through CTMT tidal forcing being closer to that observed. This is likely related to differences in tidal phase between the two models, as both models showed similar amplitudes. Analysis of the relation between TEC wave-2 enhancements and those in the integrated ion flux convergence and vertical ion drift showed that wave-2 modulation of vertical ion drift exhibited greater consistency with the TEC wave-2 during solar

maximum compared to solar minimum. This suggests that mechanisms besides tidal modulation of the E-region dynamo may also play a role in the formation of the TEC wave-2 during solar minimum.

Acknowledgments

This research was supported by grants 105-2111-M-008-001-MY3, 107-2111-M-008-002-MY3, 107-2923-M-008-001-MY3, 108-2636-M-008-002, and 109-2636-M-008-004 from the Taiwan Ministry of Science and Technology to L.C.C., as well as the Higher Education SPROUT grant to the Center for Astronautical Physics and Engineering from the Taiwan Ministry of Education. M Jones Jr. acknowledges support from the NASA Heliophysics Early Career Investigator Program. COSMIC data is available via the COSMIC Data Analysis and Archive Center (http://cdaac-www.cosmic.ucar.edu). TIE-GCM is available via the National Center for Atmospheric Research High Altitude Observatory (https://www.hao.ucar.edu/modeling/tgcm/). GSWM tidal climatologies are available at: http://www.hao.ucar.edu/modeling/gswm/gswm.html. CTMT tidal climatologies are available at: http://globaldynamics.sites.clemson.edu/articles/ctmt.html.

References

Chang, L.C., C.-H. Lin, J.-Y. Liu, B. Nanan, J. Yue, and J.-T. Lin (2013a), "Seasonal and Local Time Variation of Ionospheric Migrating Tides in 2007-2011 FORMOSAT-3/COSMIC and TIE-GCM Total Electron Content", *J. Geophys. Res. Space Physics*, 118, doi:10.1002/jgra.50268.

Chang, L. C., C.-H. Lin, J. Yue, J.-Y. Liu, and J.-T. Lin (2013b), Stationary planetary wave and nonmigrating tidal signatures in ionospheric wave 3 and wave 4 variations in 2007 - 2011 FORMOSAT-3/COSMIC observations, *J. Geophys. Res. Space Physics*, 118, 6651 - 6665, doi:10.1002/jgra.50583.

de la Beaujardière, O., The C/NOFS Definition Team (2004). C/NOFS: a mission to forecast scintillations. *J. Atmos. Sol. Terr. Phys*. 66, 1573, doi:10.1016/j.jastp.2004.07.030.

Fesen, C. G., G. Crowley, R.G. Roble, A.D. Richmond, B.G. Fejer (2000), Simulation of the pre-reversal enhancement in the low latitude vertical ion drifts, *Geophys. Res. Lett.*, 27, doi:10.1029/2000GL000061.

Forbes, J. M., X. Zhang, W. Ward, and E. R. Talaat (2002), Climatological features of mesosphere and lower thermosphere stationary planetary waves within ±40° latitude, *J. Geophys. Res.*, 107(D17), 4322, doi:10.1029/2001JD001232.

Forbes, J. M., X. Zhang, S. Palo, J. Russell, C. J. Mertens, and M. Mlynczak (2008), Tidal variability in the ionospheric dynamo region, *J. Geophys. Res.*, 113, A02310, doi:10.1029/2007JA012737.

Frissell, N. A., E. S. Miller, S. R. Kaeppler, F. Ceglia, D. Pascoe, N. Sinanis, P. Smith, R. Williams, and A. Shovkoplyas (2014), Ionospheric Sounding Using Real-Time Amateur Radio Reporting Networks, *Space Weather*, 12, 651 - 656, doi:10.1002/2014SW001132.

Fritts, D.C., and M.J. Alexander (2001), Gravity wave dynamics and effects in the middle atmosphere, *Rev. Geophys.*, 41, doi:10.1029/2001RG000106.

Gentile, L. C., W. J. Burke, P. A. Roddy, J. M. Retterer, and R. T. Tsunoda (2011), Climatology of plasma density depletions observed by DMSP in the dawn sector, *J. Geophys. Res.*, 116, A03321, doi:10.1029/2010JA016176.

Hagan, M. E., and J. M. Forbes (2002), "Migrating and nonmigrating diurnal tides in the middle and upper atmosphere excited by tropospheric latent heat release", *J. Geophys. Res.*, 107 (D24), 4754, doi: 10.1029/2001JD001236.

Hagan, M. E., and J. M. Forbes (2003), "Migrating and nonmigrating semidiurnal tides in the upper atmosphere excited by tropospheric latent heat release", *J. Geophys. Res.*, 108(A2), 1062, doi:10.1029/2002JA009466.

Häusler, K., Hagan, M. E., Forbes, J. M., Zhang, X., Doornbos, E., Bruinsma, S., and Lu, G. (2015), Intraannual variability of tides in the thermosphere from model simulations and in situ satellite observations, J. Geophys. Res. Space Physics, 120, 751– 765, doi:10.1002/2014JA020579.

Immel, T. J., E. Sagawa, S. L. England, S. B. Henderson, M. E. Hagan, S. B. Mende, H. U. Frey, C. M. Swenson, and L. J. Paxton (2006), Control of equatorial ionospheric morphology by atmospheric tides, *Geophys. Res. Lett.*, 33, L15108, doi:10.1029/2006GL026161.

Jiao, Y., and Y. T. Morton (2015), Comparison of the effect of high-latitude and equatorial ionospheric scintillation on GPS signals during the maximum of solar cycle 24, *Radio Sci.*, 50, 886 - 903, doi:10.1002/2015RS005719.

Jones, M., Jr., J.M. Forbes, M. E. Hagan, and A. Maute (2014), Impacts of vertically propagating tides on the mean state of the ionosphere-thermosphere system, J. Geophys. Res. Space Physics, 119, 2197–2213, doi:10.1002/2013JA019744.

Kelly, M. A., J. M. Comberiate, E. S. Miller, and L. J. Paxton (2014), Progress toward forecasting of space weather effects on UHF SATCOM after Operation Anaconda, *Space Weather*, 12, 601 - 611, doi:10.1002/2014SW001081.

Lin, C. H., C. H. Liu, J. Y. Liu, C. H. Chen, A. G. Burns, and W. Wang (2010), ÒMid-latitude summer nighttime anomaly of the ionospheric electron density observed by FORMOSAT-3/COSMICÓ, *J. Geophys. Res.*, 115, A03308, doi:10.1029/2009JA014084.

Liu, H.-L., and A. D. Richmond (2013), Attribution of ionospheric vertical plasma drift perturbations to large-scale waves and the dependence on solar activity, *J. Geophys. Res. Space Physics*, 118, 2452 - 2465, doi:10.1002/jgra.50265.

Moraes, A. O., E. Costa, E. R. de Paula, W. J. Perrella, and J. F. G. Monico (2014), Extended ionospheric amplitude scintillation model for GPS receivers, *Radio Sci.*, 49, 315 - 329, doi:10.1002/ 2013RS005307.

Oberheide, J., J. M. Forbes, K. Hasler, Q. Wu, and S. L. Bruinsma (2009), Tropospheric tides from 80 to 400 km: Propagation, interannual variability, and solar cycle effects, J. Geophys. Res., 114, D00I05, doi:10.1029/2009JD012388.

Oberheide, J., J. M. Forbes, X. Zhang, and S. L. Bruinsma (2011), Climatology of upward propagating diurnal and semidiurnal tides in the thermosphere, *J. Geophys. Res.*, 116, A11306, doi:10.1029/2011JA016784.

Richmond, A. D., E. C. Ridley, and R. G. Roble (1992), ÒA thermosphere/ionosphere general circulation model with coupled electrodynamicsÓ, *Geophys. Res. Lett.*, 19(6), 601 - 604, doi:10.1029/92GL00401.

Roble, R. G., E. C. Ridley, A. D. Richmond, and R. E. Dickinson (1988), "A coupled thermosphere/ionosphere general circulation model", *Geophys. Res. Lett.*, 15(12), 1325 - 1328, doi:10.1029/GL015i012p01325.

Smith, J. M., F. S. Rodrigues, B. G. Fejer, and M. A. Milla (2015), Coherent and incoherent scatter radar study of the climatology and day-to-day variability of mean F region vertical drifts and equatorial spread F, *J. Geophys. Res. Space Physics*, 121, 1466 - 1482, doi:10.1002/2015JA021934.

Smith, J., and R. A. Heelis (2017), Equatorial plasma bubbles: Variations of occurrence and spatial scale in local time, longitude, season, and solar activity, *J. Geophys. Res. Space Physics*, 122, doi:10.1002/2017JA024128.

Sultan, P. J. (1996), Linear theory and modeling of the Rayleigh-Taylor instability leading to the occurrence of equatorial spread F, *J. Geophys. Res.*, 101(A12), 26875 - 26891, doi:10.1029/96JA00682.

Tsunoda, R. T. (1985), Control of the seasonal and longitudinal occurrence of equatorial scintillations by the longitudinal gradient in integrated E region Pedersen conductivity, *J. Geophys. Res.*, 90, 447 - 456.

Tsunoda, R. T., T. T. Nguyen, and M. H. Le (2015), Effects of tidal forcing, conductivity gradient, and active seeding on the climatology of equatorial spread F over Kwajalein, *J. Geophys. Res. Space Physics*, 120, 632 - 653, doi:10.1002/2014JA020762.

Xiong, C., C. Stolle, and H. Lühr (2016), The Swarm satellite loss of GPS signal and its relation to ionospheric plasma irregularities, *Space Weather*, 14, 563 - 577, doi:10.1002/2016SW001439.

Yokoyama, T., H. Shinagawa, and H. Jin (2014), Nonlinear growth, bifurcation and pinching of equatorial plasma bubble simulated by three-dimensional high-resolution bubble model, *J. Geophys. Res. Space Physics*, 119, 10,474 - 10,482, doi:10.1002/2014JA020708.